Available online at www.sciencedirect.com

SciVerse ScienceDirect

Ceramics International 39 (2013) 1853–1861

CERAMICS INTERNATIONAL

www.elsevier.com/locate/ceramint

Investigation of the structure and the magnetic behavior of nanostructure $Ca_{1-x}Gd_xMnO_3$ ($x=0.05$; 0.1; 0.15; 0.2) obtained by modified glycine nitrate procedure

Milena Rosić[a,*], Mihovil Logar[b], Jelena Zagorac[a], Aleksandar Devečerski[a], Adela Egelja[a], Vladan Kusigerski[c], Vojislav Spasojević[c], Branko Matović[a]

[a]*Laboratory for Material Science, Institute of Nuclear Sciences "Vinča", University of Belgrade, P.O. Box 522, 11001 Belgrade, Serbia*
[b]*Faculty of Mining and Geology, University of Belgrade, Đušina 7, 11000 Belgrade, Serbia*
[c]*Condensed Matter Physics Laboratory, Institute of Nuclear Sciences "Vinča", University of Belgrade, P.O. Box 522, 11001 Belgrade, Serbia*

Received 6 July 2012; received in revised form 9 August 2012; accepted 10 August 2012
Available online 18 August 2012

Abstract

The synthesis, crystal structure and magnetic properties of $Ca_{1-x}Gd_xMnO_3$ ($x=0.05$; 0.1; 0.15; 0.2) perovskite has been investigated. Powders with nominal compositions $Ca_{0.95}Gd_{0.05}MnO_3$, $Ca_{0.9}Gd_{0.1}MnO_3$, $Ca_{0.85}Gd_{0.15}MnO_3$ and $Ca_{0.8}Gd_{0.2}MnO_3$ were prepared using a modified glycine nitrate procedure. Obtained powders were calcinated in the temperature interval from 850 °C to 950 °C for 10 min. All samples where characterized by DTA, XRD and SQUID magnetometry. The possibility of incorporation of Gd ions in the positions A of the perovskite structure was investigated by X-ray methods. Influence of Gd on unit cell volume of the perovskite compounds, occupation numbers and distances between atoms were analyzed by Rietveld refinement. Microstructure size–strain analysis was performed, as well. The results revealed that Gd entered positions A in the structure. Magnetic measurements showed that a Gd^{3+} substituted Ca^{2+} ions changes antiferromagnetic properties of $CaMnO_3$ by introduction of ferromagnetic interaction due to a double exchange between Mn^{3+} and Mn^{4+} ions.

Keywords: A. Powders: chemical preparation; B. X-ray methods; C. Magnetic properties; Spin glasses

1. Introduction

Nanoparticles and their assemblies are expected to have numerous applications in materials science. They should exhibit a range of physical and chemical properties that are promising for potential application in a new generation of optical, electronic, chemical, and biological devices [1].

Nanoparticles are typically defined as being less than 100 nm in all three dimensions. More often, they are made to be spherical having diameters on the order of 10 nm or less. At these length scales, a large fraction of the particle's atoms are at or near the surface providing them with unique properties. In the case of magnetic nanoparticles, crystal symmetry breaking at the surface has profound ramifications. The specific advantages of the nanopowders include superior phase homogeneity and lower densification temperature. Beyond achieving nanoscaled particles, the control of other powder characteristics such as particle distribution, phase purity, and morphology are equally important in obtaining promising performance [2].

There are numerous reported synthetic methods for the production of nanoparticles [3]. The challenge is to control the nanoparticle size, size distribution, morphology, crystallinity, shape, and properties, to assemble the nanoparticles for a given purpose, and to make them from a variety of materials.

Nanoscaled particles agglomerate easily due to the very strong van der Waals attraction force between small particles. The aggregate acts as a single particle and is difficult to be broken up due to its strong bonding force [4].

*Corresponding author. Tel./fax: +381 11 3408 224.
E-mail address: mrosic@vinca.rs (M. Rosić).

0272-8842/$ - see front matter © 2012 Elsevier Ltd and Techna Group S.r.l. All rights reserved.
http://dx.doi.org/10.1016/j.ceramint.2012.08.033

Therefore, chemical processing methods such as modified glycine nitrate procedure have been studied to prepare ultrafine, $Ca_{1-x}Gd_xMnO_3$ ($x=0.05$; 0.1; 0.15; 0.2) powders.

The magnetism in oxide systems stems from double-exchange and/or superexchange interactions, both of which are very sensitive to the bond angles that form between cation–anion–cation arrangements. Surface bond-bending in these cases leads to profound changes in the magnetic interactions, in some instances changing its behavior from ferromagnetism to antiferromagnetism or to a spin glass-like behavior [5].

From the magnetic viewpoint, the nanoparticle manganites usually exhibit qualitatively new properties in respect to their bulk counterparts, such as changes in magnetic transition temperatures, the emergence of superparamagnetism, size dependence of the saturation magnetization and coercivity, etc. [6–8].

The structure of manganites is governed by the Goldschmidts tolerance factor $f=(r_A+r_O)/\sqrt{2}(r_B+r_O)$ [9]. Goldschmidts tolerance factor for $Ca_{1-x}Gd_xMnO_3$ ($x=0.05$; 0.1; 0.15; 0.2) nanopowders are shown in Table 1. It is in the range of 1.00637–0.99018, which leads us to the conclusion that observed nanometric structures could be stable.

Today, the experimental data on gadolinium-doped manganites available in the literature are limited and not conclusive in various aspects. Several papers [10–13], have been published for the studies of $CaMnO_3$ doped with Gd and its structure and electrical and magnetic properties have been investigated in detail. However, all these works are not related to nanopowders $Ca_{1-x}Gd_xMnO_3$ ($x=0.05$; 0.1; 0.15; 0.2), but bulk materials and used Gd as a dopant in a larger percentage.

The goal of the present work is to present structural and magnetic properties of nanoparticled $Ca_{1-x}Gd_xMnO_3$ system which is exploring in our laboratory for several years. We focus on its chemical synthesis by glycine nitrate method and present evolution of its antiferromagnetic properties upon different Gd^{3+} doping ranging from $x=0.05$ to $x=0.20$.

2. Experimental

Starting chemicals used for the synthesis of powders were aminoacteic acid–glycine (Fischer Scientific, USA), Mn-acetate ($Mn(CH_3CO_2)_2\cdot 4H_2O$), Mn-nitrate ($Mn(NO_3)_2\cdot H_2O$), Ca-nitrate ($Ca(NO_3)_2\cdot 4H_2O$) and Gd-nitrate ($Gd(NO_3)_3\cdot 6H_2O$), supplied by Aldrich, USA. The compositions of reacting mixtures were calculated according to the principle of propellant chemistry [14]. By convention, the valencies of carbon, nitrogen, oxygen, hydrogen, gadolinium, calcium and manganese are set as 4+, 0, 2−, 1+, 3+, 2+, and 2+, respectively. Using the valencies of these individual elements, the net oxidizing valency of $Gd(NO_3)_3$, $Ca(NO_3)_2$, $Mn(NO_3)_2$, and $Mn(CH_3CO_2)_2$ works out to be 15−, 10−, 10−, and 16+, respectively, where as the reducing valency of glycine works out to be 9+.

Hence, required moles of glycine for producing one mole of $Ca_{1-x}Gd_xMnO_3$ ($x=0.05$; 0.1; 0.15; 0.2) nanopowders through the stochiometric reaction are shown in Table 2.

Preparation of $Ca_{1-x}Gd_xMnO_3$ ($x=0.05$; 0.1; 0.15; 0.2) powders were performed according to reactions:

$$C_2H_5NO_2+0.5Mn(CH3CO2)_2\cdot 4H_2O+0.95Ca(NO_3)_2\cdot 4H_2O+0.5Mn(NO_3)_2\cdot H_2O+0.05Gd(NO_3)_3\cdot 6H_2O+0.975O_2\rightarrow Ca_{0,95}Gd_{0,05}MnO_3+2CH_3COOH+4.05NO_2\uparrow+6.6H_2O \quad (1)$$

$$C_2H_5NO_2+0.5Mn(CH3CO2)_2\cdot 4H_2O+0.9Ca(NO_3)_2\cdot 4H_2O+0.5Mn(NO_3)_2\cdot H_2O+0.1Gd(NO_3)_3\cdot 6H_2O+0.95O_2\rightarrow Ca_{0,9}Gd_{0,1}MnO_3+2CH_3COOH+4.1NO_2\uparrow+6.7H_2O \quad (2)$$

$$C_2H_5NO_2+0.5Mn(CH3CO2)_2\cdot 4H_2O+0.85Ca(NO_3)_2\cdot 4H_2O+0.5Mn(NO_3)_2\cdot H_2O+0.15Gd(NO_3)_3\cdot 6H_2O+0.925O_2\rightarrow Ca_{0,85}Gd_{0,15}MnO_3+2CH_3COOH+4.15NO_2\uparrow+6.8H_2O \quad (3)$$

$$C_2H_5NO_2+0.5Mn(CH3CO2)_2\cdot 4H_2O+0.8Ca(NO_3)_2\cdot 4H_2O+0.5Mn(NO_3)_2\cdot H_2O+0.2Gd(NO_3)_3\cdot 6H_2O+0.9O_2\rightarrow Ca_{0,8}Gd_{0,2}MnO_3+2CH_3COOH+4.2NO_2\uparrow+6.9H_2O \quad (4)$$

On the basis of calculations according to the principle of propellant chemistry and four reaction models presented by Eqs.(1–4), four different samples were obtained.

Synthesis was carried out in a stainless steel reactor in which all reactants dissolved in distilled water were added according to previously calculated composition of the final powder. Hence, when dissolved in water, initially it forms a heterogeneous medium where the reaction takes place at the interface [15].

Table 1
A Goldschmidts tolerance factor for $Ca_{1-x}Gd_xMnO_3$ ($x=0.05$; 0.1; 0.15; 0.2) nanopowders.

$Ca_{1-x}Gd_xMnO_3$	Goldschmidts tolerance factor f
$Ca_{0.95}Gd_{0.05}MnO_3$	1.00637
$Ca_{0.9}Gd_{0.1}MnO_3$	1.00097
$Ca_{0.85}Gd_{0.15}MnO_3$	0.99557
$Ca_{0.8}Gd_{0.2}MnO_3$	0.99018

Table 2
Required moles of glycine for producing one mole of $Ca_{1-x}Gd_xMnO_3$ ($x=0.05$; 0.1; 0.15; 0.2) nanopowders through the stochiometric reaction.

1 mol $Ca_{1-x}Gd_xMnO_3$	Required moles of glycine
$Ca_{0.95}Gd_{0.05}MnO_3$	0.8056
$Ca_{0.9}Gd_{0.1}MnO_3$	0.8333
$Ca_{0.85}Gd_{0.15}MnO_3$	0.8611
$Ca_{0.8}Gd_{0.2}MnO_3$	0.8889

Thermal properties have been investigated using the modernized furnace, Chevenard Joimer Instrument A.D.A.M.E.L [16] equipped with Pt-PtRh thermocouples together with the digital data acquisition computer system. The t and Δt voltages were collected over the 16-bit USB-2523 AD converter with 1 Hz sampling rate. The heating rate was 8 °C/min. Consequently in the temperature range of 20 °C–1000 °C around 7350 points were read. The reference material used was α-Al_2O_3. Simultaneous DTA of each reaction was carried out to study the decomposition behavior and nature of the combustion reaction. On the basis of DTA analysis it is found that the resulting amorphous powders crystallize in the temperature range from 880 °C to 955 °C. In this manner, it was established calcination temperature (Nabertherm furnaces).

The phases of samples were identified using X-ray powder diffraction (XRPD) on a SiemensD500 diffractometer with a Ni filter using Cu K_α radiation and the step-scan mode (2θ-range: 10°–80° in a continuous scan mode with a step width of 0.02° and 0.5 s/step). To derive the relevant structural parameters, the experimental data for Rietveld refinement were taken afterwards over an angular range 10°–105° 2θ, with a step width of 0.03° and 14 s/step. Structural analysis was carried out using Rietveld refinement and the program FullProf [17–19].

Magnetic properties were measured by the Quantum Design SQUID magnetometer MPMS XL-5. Temperature dependence of magnetization M(T) was measured in both zero-field cooled (ZFC) and field cooled (FC) regime, in two different magnetic fields of 100 Oe and 1000 Oe. Magnetization dependence on magnetic field strength M(H) was measured at temperatures below and above phase transition temperatures. AC magnetic susceptibility was recorded at two frequencies (10 Hz and 1000 Hz), with 4 Oe driving amplitude, in the temperature range encompassing spin-glass (SG) and antiferromagnetic–paramagnetic (AF–P) phase transitions.

3. Results and discussion

3.1. DTA

Fig. 1 shows the DTA curves for the synthesized powder of $Ca_{1-x}Gd_xMnO_3$ (x=0.05; 0.1; 0.15; 0.2). The thermal decompositions are described by the existence of three main degradation stages (endotherm, exotherm and endotherm, respectively). As shown in Fig. 1 the first one, starts from 87 °C to 144 °C corresponding to the elimination of absorbed water in the powder. This decomposition stage consists in an initial very weak endothermic effect (~140 °C, shoulder) representing water evolving, followed by a fast and intensive exothermic process (second stage), consisting in simultaneous evolving of NO_3^- and glycine. Simultaneously, glycine is oxidized by nitrate anions [20]. Sharp exothermic peaks were found in two cases (curves (c) and (d) on Fig. 1), which indicates the occurrence of combustion reaction. The exothermal peaks

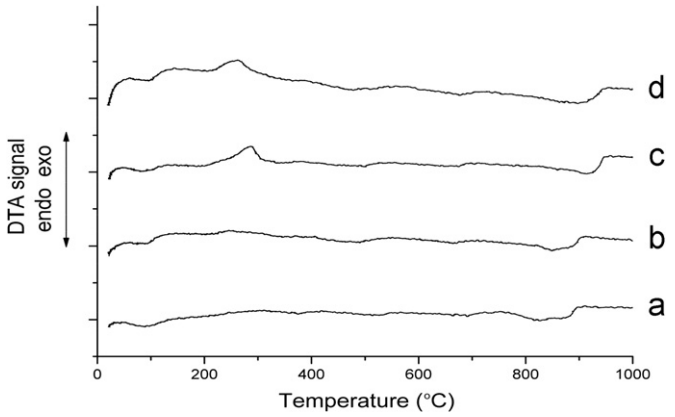

Fig. 1. DTA diagrams of synthesized $Ca_{1-x}Gd_xMnO_3$ (x=0.05; 0.1; 0.15; 0.2) powders: (a) $Ca_{0.95}Gd_{0.05}MnO_3$; (b) $Ca_{0.9}Gd_{0.1}MnO_3$; (c) $Ca_{0.85}Gd_{0.15}MnO_3$; (d) $Ca_{0.8}Gd_{0.2}MnO_3$.

at 262 °C and 285 °C indicate the decomposition and decarbonization of the residue organic compounds in the powder, respectively [21]. The endothermic DTA peak observed around 478 °C and 514 °C can be attributed to the chemical change from MnO_2 to Mn_2O_3 in this structural change [22]. Therefore, the second decomposition stage, accompanied by a medium exothermic effect, represents the burn up of the remainder carbonaceous residue and interaction due to a double exchange between Mn^{3+} and Mn^{4+} ions [23]. The exothermic peak associated with the anion decomposition reaction was 675 ± 3 °C, confirming that nitrate breakdown occurred in a melt [24]. The third stage shows an initial weak endothermic effect (910 °C–960 °C) representing the onset of crystallization.

Based on the DTA results the powders prepared by glycine route have been calcined at temperature range from 900 °C to 960 °C for 10 min. The results indicate that intimate mixing on the atomic level of the oxidant and the fuel in the form of a stable gel is necessary for the propagation of combustion reaction.

3.2. Powder XRD

After combustion reaction the XRD patterns of the obtained powders (not shown) were found to be amorphous in nature possibly due to insufficient heat generated during auto-ignition. The completion of the reaction and the phase purity of the samples were confirmed by powder X-ray diffraction methods. The XRD patterns reflected the presence of a mono-phasic $Ca_{1-x}Gd_xMnO_3$ (x=0.05; 0.1; 0.15; 0.2) perovskite. The best fits between calculated and observed X-ray diffraction patterns for samples $Ca_{1-x}Gd_xMnO_3$ (x=0.05; 0.1; 0.15; 0.2) are given in Fig. 2. All allowed Bragg reflections are shown by vertical bars. According to X-ray measurements, the XRD patterns of all powders looked similar to each other, despite the different amount of dopant. However, a slight difference of peak widths as well as the shifting the peaks toward

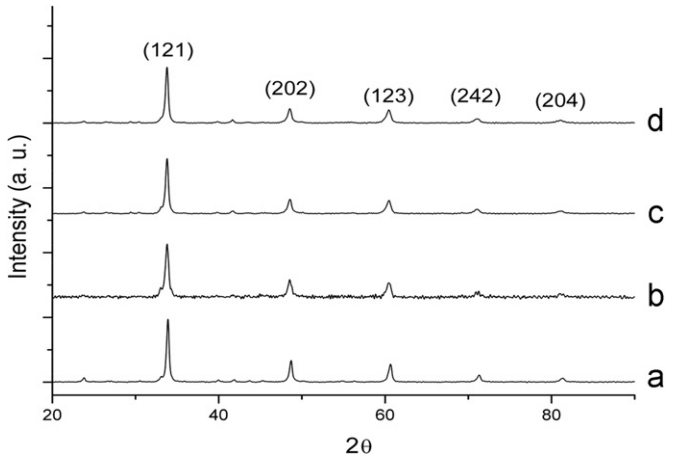

Fig. 2. XRD patterns of $Ca_{1-x}Gd_xMnO_3$ ($x=0.05$; 0.1; 0.15; 0.2) powders:. (a) $Ca_{0.95}Gd_{0.05}MnO_3$; (b) $Ca_{0.9}Gd_{0.1}MnO_3$; (c) $Ca_{0.85}Gd_{0.15}MnO_3$; (d) $Ca_{0.8}Gd_{0.2}MnO_3$.

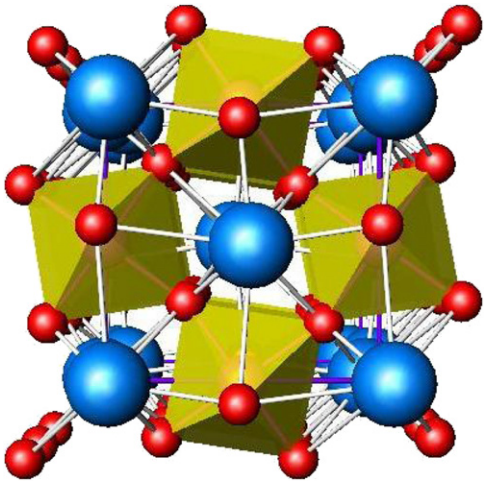

Fig. 3. Crystal structure of $Ca_{1-x}Gd_xMnO_3$.

lower angles with increasing dopant amounts were observed. By inspecting difference between the experimental and calculated profiles, good agreement can be observed. All peaks are broad and with low intensities indicating nano-crystalline nature of the powders.

From the refinement of the structure analysis by the Rietveld method using powder X-ray diffraction data, it was derived that all the samples are assigned to be single-phase of the orthorhombic-perovskite structure described by *Pnma* space group and its structure is given in Figs. 3 and 4. Tables 3 and 4 present results of the Rietveld analysis, i.e., unit cell parameters, unit cell volume, microstructure parameters and atomic positions.

The structure was described with (Ca, Gd) atoms located at *4c* positions, Mn atoms at *4b*, and oxygen atoms at *4c* and *8d* positions. The results of Rietveld refinement clearly demonstrated that in the case of Gd doped solid solutions the cations occupied A site. The data from Ref. [25] were used as the starting model for refinement that indicated the presence of dopants in the structure. This Gd^{3+} presence in the structure, causes the reduction of Mn^{4+} into Mn^{3+}, because substituting the Ca site with a trivalent cation Gd^{3+} induces Mn^{3+} cation in Mn^{4+} matrix, whose ionic radius is larger than that of Mn^{4+} (0.645 Å for Mn^{3+} and 0.530 Å for Mn^{4+}, respectively) and cause the increase of unit cell volume. The Table 3 shows that it increases concentrations of gadolinium in the structure, and to increase their unit cell volume.

Line-broadening analysis was performed using the Rietveld method in conjunction with Warren–Averbach procedure in order to get crystallite size and lattice microstrain parameters. In the present approach, the grain size broadening was represented by a Lorentzian function, and micro-strain broadening by a Gaussian function. The convolution of these functions is a pseudo-Voigt function which is approximated by a modified Thompson–Cox–Hastings pseudo-Voigt [26]. In addition, all obtained powders show that crystallite sizes are in nanometric range, about 26 nm–35 nm.

Table 4 presents beside atomic positions, the variation in average Mn–O bond length as a function of average A-site ionic radii and suggests the structural distortions because of presence of Gd^{3+} and Mn^{3+} in the structure.

3.3. Magnetic properties

Temperature dependence of magnetization, for all Gd concentrations, recorded in the magnetic field of 100 Oe, and in the temperature range from 5 K to 300 K, is depicted in Fig. 5. All $M(T)$ curves show very slow increase of magnetization when temperature decreases from 300 K to about 130 K and then, an abrupt increase of magnetization is appreciable. Similar increase is noticed in all manganites where Ca^{2+} molar fraction $x>0.5$ and it can be assigned to AF–P phase transition [21,27]. Néel temperature T_N about 110 K, which is almost independent on Gd concentration, was determined from dM/dT derivate (not shown). Below T_N very high irreversibility, between ZFC and FC branches (empty and full symbols, respectively) is visible.

FC branches, for all Gd concentrations, continually increase showing plateau below 30 K, but for the lowest temperatures additional increase in both, FC and ZFC curves, is observed. This magnetization increase below T_N accompanied with plateau at low temperatures is characteristic for ferromagnetics. It is well known that FM component in mixed valence manganite arise from double exchange interactions between Mn^{3+} and Mn^{4+} ions [28]. Mixed valence of manganese ions appear after Gd^{3+} doping (electron doping), as a consequence of electroneutrality preservation. Gd^{3+} ions replace Ca^{2+} at A site position, but their fraction is too low to build long range magnetic order. Instead of this, due to Mn^{3+}–Mn^{4+} exchange interactions, short range ordering occurs, forming FM clusters in the AF matrix. FM order in clusters and AF interaction in background is main reason of frustration which is occurring in this system. It can be also noticed that at low temperatures magnetization

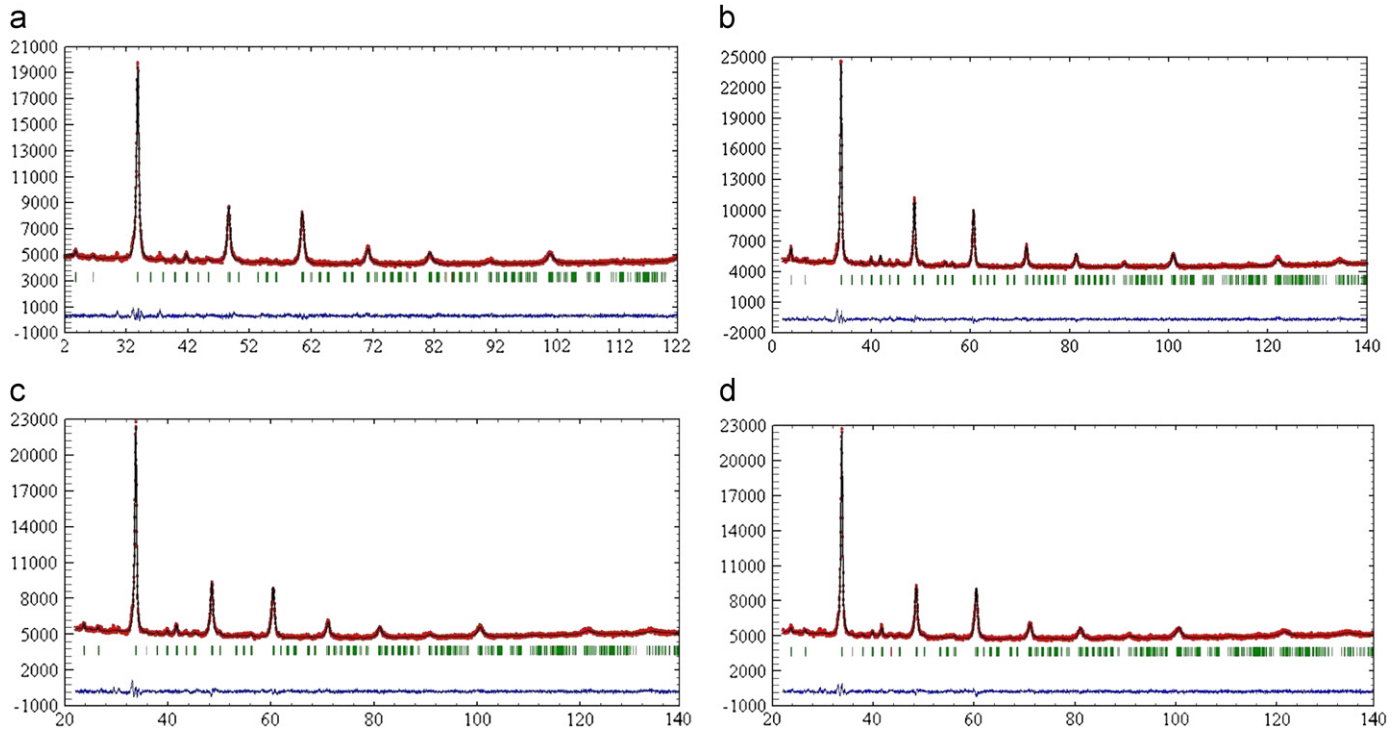

Fig. 4. Results of Rietveld refinement of the samples: (a) $Ca_{0.95}Gd_{0.05}MnO_3$; (b) $Ca_{0.9}Gd_{0.1}MnO_3$; (c) $Ca_{0.85}Gd_{0.15}MnO_3$; (d) $Ca_{0.8}Gd_{0.2}MnO_3$.

Table 3
Results of Rietveld refinement.

	Sample			
	$Ca_{0.95}Gd_{0.05}MnO_3$	$Ca_{0.9}Gd_{0.1}MnO_3$	$Ca_{0.85}Gd_{0.15}MnO_3$	$Ca_{0.8}Gd_{0.2}MnO_3$
Unit cell parameters (Å)	$a=5.2834(5)$, $b=7.4665(6)$, $c=5.2994(4)$	$a=5.304(1)$, $b=7.475(1)$, $c=5.293(1)$	$a=5.3152(9)$, $b=7.4795(8)$, $c=5.303(1)$	$a=5.3186(5)$, $b=7.4792(7)$, $c=5.3003(7)$
Volume (Å^3)	$V=209.03(3)$	$V=209.84(7)$	$V=210.81(6)$	$V=210.84(7)$
Microcrystalline size (Å)	259.3(2)	303.6(1)	254.2(5)	354.0(5)
Microstrain	0.01538	0.03431	0.03129	0.04157

increases with Gd concentration reaching maximum for 0.15, and then decreases for $x=0.20$.

On the other hand, ZFC branches show the decrease of magnetization with additional maximums at $T_{SG} \approx 55$ K (Fig. 4. inset). These peaks are typical for spin-glasses and occur as a consequence of frustration between short range—ferromagnetic and long range—antiferromagnetic interactions. With the increase of concentration x, these maximums become more pronounced and reach maximal intensity, like in FC branches, for $x=0.15$.

Increase of magnetization which is visible in both ZFC and FC branches for $T<10$ K can be assign to the large contribution of Gd^{3+} paramagnetic moments ($\mu_{Gd}^{3+}=7.94$ μ_B [29]) which is particularly pronounced at low temperatures. This contribution can be calculated according to the Langevin theory, where magnetization per mol of $Ca_{1-x}Gd_xMnO_3$ can be expressed as

$$M = xN_A J g_J \mu_B B_J(\eta) \quad (5)$$

$$B_J(\eta) = (2J+1)/2J \coth[(2J+1)\eta/2J] - 1/2J \coth(\eta/2J)$$

$$\eta = J g_J \mu_B B/k_B T$$

$B_J(\eta)$ is Brillouin function, N_A is Avogadro's number, $g_J=2$ is Landé factor, and $J=7/2$ is quantum number of angular moment. The contribution of Gd^{3+} ions to the magnetization of $Ca_{0.8}Gd_{0.2}MnO_3$ is depicted in the Fig. 6. (open squares), while corrected $M(T)$ values (after subtraction of Gd^{3+} paramagnetic contribution) is represented by the solid line. It is visible that Gd^{3+} contribution is especially pronounced at low temperatures where it can change the flow of $M(T)$ curve.

The $M(T)$ plateau at low temperatures is characteristic for FM interaction, but the decrease of magnetization, which is appeared after subtraction of Gd^{3+} paramagnetic contribution, shows that still AF interaction is present, what is the main reason for frustration of interactions and the arising of spin-glass state.

Table 4
Refined atomic parameters results.

	Sample			
	$Ca_{0.95}Gd_{0.05}MnO_3$	$Ca_{0.9}Gd_{0.1}MnO_3$	$Ca_{0.85}Gd_{0.15}MnO_3$	$Ca_{0.8}Gd_{0.2}MnO_3$
Ca (Gd)				
x	0.0305(7)	0.0253(9)	0.0300(8)	0.0298(7)
y	0.25	0.25	0.25	0.25
z	−0.01(1)	−0.01(2)	−0.011(1)	−0.01(1)
Occ (%)				
Ca	0.464(1)	0.442(2)	0.431(2)	0.441(2)
Gd	0.036(1)	0.058(2)	0.069(2)	0.059(2)
Mn site				
x	0.5	0.5	0.5	0.5
y	0	0	0	0
z	0	0	0	0
O1 site				
x	0.490(3)	0.482(4)	0.488(4)	0.493(3)
y	0.25	0.25	0.25	0.25
z	0.061(2)	0.076(3)	0.071(4)	0.054(3)
O2 site				
x	0.298(3)	0.304(2)	0.295(3)	0.305(3)
y	0.028(2)	0.025(2)	0.017(3)	0.021(3)
z	−0.289(2)	−0.286(3)	−0.289(3)	−0.295(3)
Mn–O	1.8978(10)	1.84859(5)	1.90684(3)	1.88364(4)
	1.9335(9)	1.97726(6)	1.91820(3)	1.96677(4)
	1.8978(10)	1.84859(5)	1.90684(3)	1.88364(4)
	1.9335(9)	1.97726(6)	1.91820(3)	1.96677(4)
	1.8994(7)	1.91378(5)	1.90151(2)	1.91264(3)
	1.8994(7)	1.91378(5)	1.90151(2)	1.91264(3)

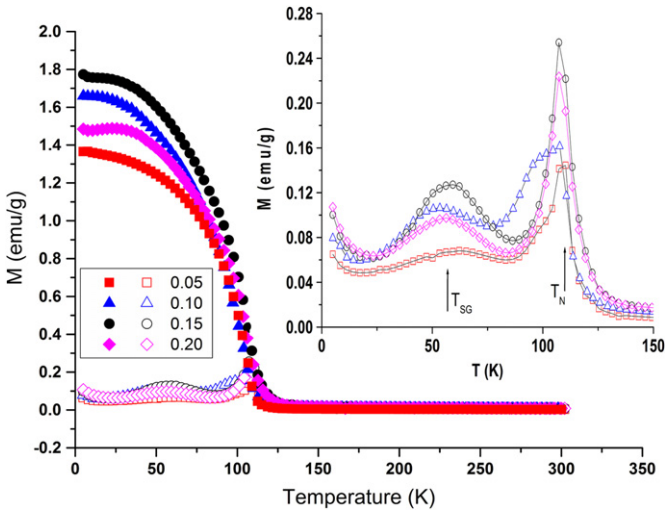

Fig. 5. Temperature dependence of ZFC (open symbols) and FC magnetization (full symbols) of $Ca_{1-x}Gd_xMnO_3$ in the magnetic field of 100 Oe. Inset: Details of ZFC magnetization; spin-glass transition and Néel temperature are denoted by arrows.

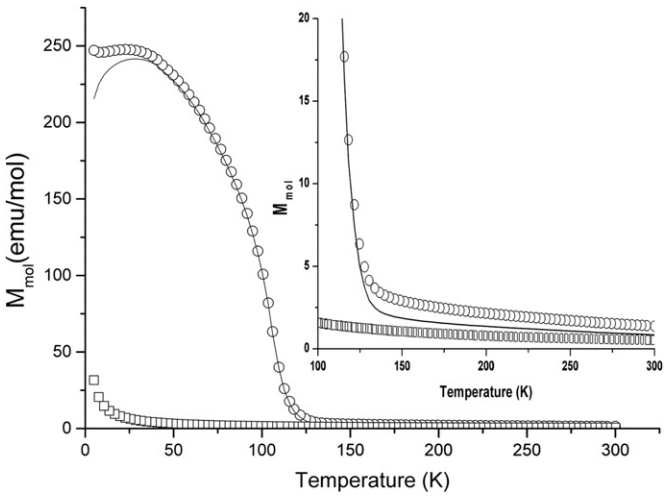

Fig. 6. Temperature dependence $Ca_{0.8}Gd_{0.2}MnO_3$ magnetization (open circles), calculated paramagnetic contribution of Gd^{3+} ion (open squares), M(T) after subtracting Gd^{3+} contribution (solid line). Inset: Details of $M(T)$ at higher temperatures.

The paramagnetic Gd^{3+} contribution at higher temperatures is presented in the inset of the same figure (open squares), where corrected values of magnetization are depicted by the solid line. This contribution is important to account when high temperature magnetic susceptibility data are fitted by using the Curie–Weiss law. In this way obtained effective magnetic moments μ_{eff} and paramagnetic Curie–Weiss temperature θ are depicted in Fig. 7.

It can be noticed that μ_{eff} increases with concentration of Gd^{3+} ion x, following linear dependence $\mu_{eff}(x)=0.82x+3.88$

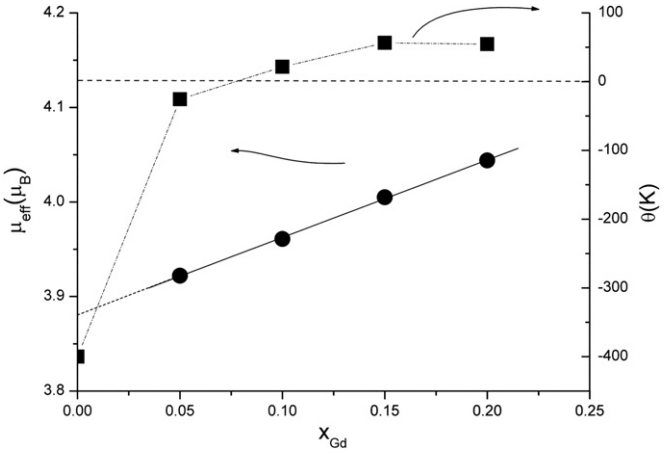

Fig. 7. Concentration dependence of effective magnetic moment μ_{eff} and Curie–Weiss temperature θ for $Ca_{1-x}Gd_xMnO_3$ (θ values for $x=0$ are taken from [28]).

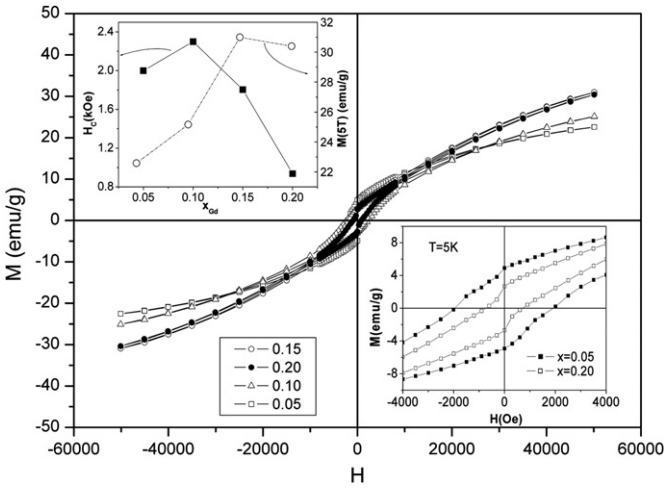

Fig. 8. Hysteresis curves of $Ca_{1-x}Gd_xMnO_3$ at 5K. Insets: below-details for $x=0.05$ and $x=0.20$; above-coercitivity vs. concentration.

(solid line in Fig. 6.). Values of 3.88 μ_B and 4.70 μ_B obtained by extrapolation for $x=0$ and 1 are in accordance with spin-only values 3.87 μ_B and 4.90 μ_B for Mn^{4+} and Mn^{3+} ions, respectively. If we write chemical formula for this compound as $Ca_{1-x}Gd_xMn^{3+}_{1-y}Mn^{4+}_yO_3$, then contributions to the μ_{eff} of both Mn ions with different valence states can be estimated from:

$$\mu^2_{eff} = y\mu^2_{Mn^{3+}} + (1-y)\mu^2_{Mn^{4+}}. \quad (6)$$

The y values, obtained from the expression (6) shows that Mn^{4+}/Mn^{3+} ratio is close to Ca^{2+}/Gd^{3+} one, speaking in favor of a good stoichiometry with the possible excess of oxygen not higher then $\delta=0.04$.

The same figure shows that Curie–Weiss temperature starts from negative θ value, which is characteristic for antiferromagnetic $CaMnO_3$ ($x=0$) and reaches positive value for $x>0.05$. Similar $\theta(x)$ dependence has been found in polycrystalline $Y_xCa_{1-x}MnO_3$ and $La_xCa_{1-x}MnO_3$ [30], where paramagnetic Curie–Weiss temperature changes negative sign to positive above certain concentration x. Such behavior of Curie–Weiss temperatures can be explained by the evolution of magnetic structure upon electron doping. Neutron diffraction experiments on electron doped manganites showed an evolution of magnetic structure [31]. The "pure" $CaMnO_3$ has magnetic structure of an antiferromagnetic of G-type [32], where magnetic moments on every neighboring Mn^{4+} cations are aligned oppositely to each other. In order to preserve electroneutrality, doping of Gd^{3+} at A crystallographic sites causes creation of Mn^{3+} ions at B sites generating the mixed valence manganites. By increasing concentration x, G-type magnetic structure is gradually changing to an antiferromagnetic phase of C-type. This type of magnetic structure is characterized by the one-dimensional chains of parallel ordered Mn moments (FM interaction), but neighboring chains are antiparallely oriented (AF interaction) [32]. The FM exchange interaction along the chains is short-range and arises from double exchange mechanism between Mn^{3+} and Mn^{4+}. On the other hand, AF superexchange interaction which acts between the chains is the long range one. By increasing concentration x, number of Mn^{3+} ions is increasing and consequently increases probability for forming FM clusters which are dispersed in the AF matrix. Consequences of this process are increase of effective magnetic moment μ_{eff} and positive values of Curie–Weiss temperature θ.

Hysteresis curves of $Ca_{1-x}Gd_xMnO_3$ at $T=5$ K, after subtraction of paramagnetic Gd^{3+} contribution according to Eq. (5), are depicted in the Fig. 8. It can be seen that for $T=5$ K magnetization does not saturate even for 50 kOe due to the existence of antiferromagnetic interactions. Starting from lower concentration x magnetization at 5 K abruptly increases reaching maximum for $x_{max}=0.15$ and then slightly decreases for 0.20 (inset above). On the other hand coercitivity reaches the highest value of $H_c=2300$ Oe for $x=0.10$, and then drops to 750 Oe for $x=0.20$. Similar $M(x)$ and $H_c(x)$ dependence behavior is reported in several manganites. For example, systematic study performed at polycrystalline $Ln_xCa_{1-x}MnO_3$ (Ln=La, Nd, Gd, Y), in the wide range of $x=0.02$–0.25, showed that all substances showed similar dependence of magnetic moments vs. concentration x with $x_{max}=0.08$ for La and Nd, 0.10 for Gd, and 0.15 for Y [33]. Above concentration x_{max} an abrupt decrease of magnetic moments were detected. To our best knowledge in nanoparticled counterparts, similar behavior was described only in nanocrystalline $La_xCa_{1-x}MnO_3$, where instead of sharp maximum at certain concentration x_{max} magnetization displays broad maximum in the concentration range from 0.10 to 0.18 [34].

Hysteresis loops were also measured in polycrystalline $La_xCa_{1-x}MnO_3$ in the concentration region $x<0.10$ [33]. It was found, like in our case, that the samples with the lower lanthanum concentration ($x\leq 0.06$) showed significantly higher coercitivity then the sample with $x=0.08$.

This $M(x)$ and $H_c(x)$ dependence confirm broadly accepted presupposition about existence of ferromagnetic ordered clusters in antiferromagnetic matrix. It is assumed that when the system is exposed to a magnetization reversal process, the interfacial spins between AFM and FM regions rotate but with an increased rotational drag due to interaction with AF matrix, resulting to broadening of hysteresis loop [33] i.e. to the increase of H_c. When concentration x increases, number and size of FM clusters increases leading to the magnetization increase, but in the same time, rotational drag is reducing causing decrease of coercitivity (Fig. 8, insets).

4. Conclusion

Innovative materials processing techniques, such as the modified combustion process described here, seem to hold much promise for the preparation of technologically important perovskite $Ca_{1-x}Gd_xMnO_3$, with "x" ranging from 0.05 to 0.20, owing to the control over stoichiometry, homogeneity and purity.

A major breakthrough in the investigation of this family of oxides has resulted from improved structural descriptions, such as the composite structure model, $Ca_{1-x}Gd_xMnO_3$ and the application of the space group approach towards structure determination.

The Rietveld refinement showed that the obtained powders exhibit a precise stoichiometry compared to the tailored composition. It was found that the crystallite size lies in the nanometric range (26 nm–35 nm). The calculated and measured lattice parameters and average bond distances increase with higher dopant concentration.

Magnetic measurements showed that when concentration x increases, magnetization also increases due to the formation of ferromagnetic ordered clusters in antiferromagnetic $CaMnO_3$ matrix.

Acknowledgment

This project was financially supported by the Ministry of Science and Environmental Protection of Serbia (project number: 45012).

References

[1] C.N.R. Rao, P.J. Thomas, G.U. Kulkarni, Nanocrystals Synthesis, Properties and Applications, vol. 95, Springer Series in Materials Science, 2007, pp. 1–25.
[2] J. Jortner, C.N.R. Rao, Nanostructured advanced materials. Perspectives and directions, Pure and Applied Chemistry 74 (2002) 1491–1506.
[3] T. Sugimoto, Fine Particles, Synthesis, Characterization, and Mechanisms of Growth, Marcel Dekker, New York, 2000.
[4] J.T.G. Overbeek, Colloidal Dispersions, Royal Society of Chemistry, London, 1981.
[5] R.H. Kodama, A.E. Berkowitz, E.J. McNiff, S. Foner, Surface spin disorder in $NiFe_2O_4$ nanoparticles, Physical Review Letters 77 (1996) 394–397.
[6] M. Muroi, R. Street, P.G. McCormick, Structural and magnetic properties of ultrafine $La_{0.7}Ca_{0.3}MnO_z$ powders prepared by mechanical alloying, Journal of Solid State Chemistry 152 (2000) 503–510.
[7] M. Muroi, R. Street, P.G. McCormick, Enhancement of critical temperature in fine La…Ca…MnO… particles prepared by mechanochemical processing, Journal of Applied Physics 87 (2000) 3424–3431.
[8] P. Katiyar, D. Kumar, T.K. Nath, A.V. Kvit, J. Narayan, S. Chattopadhyay, W.M. Gilmore, S. Coleman, C.B. Lee, J. Sankar, R.K. Singh, Magnetic properties of self-assembled nanoscale $La_{2/3}Ca_{1/3}MnO_3$ particles in an alumina matrix, Applied Physics Letters 79 (2001) 1327–1329.
[9] M. Mogensen, D. Lybye, N. Bonanos, P.V. Hendriksen, F.W. Poulsen, Factors controlling the oxide ion conductivity of fluorite and perovskite structured oxides, Solid State Ionics 174 (2004) 279–286.
[10] S. Hirano, J. Sugiyama, T. Noritake, T. Tani, Chemical pressure effect on magnetic properties in electron-doped perovskite manganites $(Gd_{0.08}Ca_ySr_{0.92-y})MnO_3$ $(0<y<1)$: percolation transition of ferromagnetic clusters, Physical Review B 70 (2004) 094419-1–094419-8.
[11] Y. Wang, Y. Sui, W. Su, High temperature thermoelectric characteristics of $Ca_{0.9}R_{0.1}MnO_3$ (R=La, Pr,…, Yb), Journal of Applied Physics 104 (2008) 093703-1–093703-8.
[12] L. Sudheendra, A.R. Raju, C.N.R. Rao, A systematic study of four series of electron-doped rare earth manganates, $Ln_xCa_{1-x}MnO_3$ (Ln=La, Nd, Gd and Y) over the $x=0.02$–0.25 composition range, Journal of Physics: Condensed Matter 15 (2003) 895–905.
[13] I. Medvedeva, A. Maignan, C. Martin, K. Bärner, B. Raveau, Yu. Bersenev, N. Mushnikov, E. Gerasimov, Hydrostatic pressure effect on electrical and magnetic properties of electron-doped $R_{0.16}Ca_{0.84}MnO_3$ (R=Pr, Gd, Eu), Physica B: Condensed Matter 365 (2005) 114–120.
[14] K.C. Patil, M.S. Hegde, T. Rattan, S.T. Aruna, Chemistry of Nanocrystalline Oxide Materials: Combustion Synthesis, Properties and Applications, World Scientific Publishing Co. Pte. Ltd., Singapore, 2008.
[15] S.R. Nair, R.D. Purohit, A.K. Tyagi, P.K. Sinha, B.P. Sharmaz, Low-temperature sintering of $La(Ca)CrO_3$ powder prepared through the combustion process, Journal of the American Ceramic Society 91 (2008) 88–91.
[16] A. Kostić-Pulek, S. Marinković, R. Tomanec, M. Logar, The influence of magnesium chloride concentration in the liquid phase on the hydrothermal dehydration of gypsum, Ceram.-Silik 38 (1994) 173–177.
[17] J. Rodriguez-Carvajal, FullProf Computer Program, ⟨ftp://charybde.saclay.cea.fr/pub/divers/fullprof.98/windows/winfp98.zip⟩, 1998.
[18] J. Rodríguez-Carvajal, Recent advances in magnetic structure determination by neutron powder diffraction, Physica B: Condensed Matter 192 (1993) 55–69.
[19] J Rodríguez-Carvajal, Recent developments of the program FULLPROF, in Commission on Powder Diffraction (IUCr), IUCr Newsletter 26 (2001) 12.
[20] C.H. Yan, Z.G. Xu, F.X. Xheng, Z.M. Wang, L.D. Sun, C.S. Liao, J.T. Jia, Nanophased $CoFe_2O_4$ prepared by combustion method, Solid State Communications 111 (1999) 287–291.
[21] Y.-J. Yang, T.-L. Wen, H. Tu, D.-Q. Wang, J. Yang, Characteristics of lanthanum strontium chromite prepared by glycine nitrate process, Solid State Ionics 135 (2000) 475–479.
[22] J. Philip, T.R.N. Kutty, Preparation of manganite perovskites by a wet-chemical method involving a redox reaction and their characterization, Materials Chemistry and Physics 63 (2000) 218–225.
[23] B.M. Nagabhushana, R.P.S. Chakradhar, K.P. Ramesh, C. Shivakumara, G.T. Chandrappa, Combustion synthesis, characterization and metal–insulator transition studies of nanocrystalline $La_{1-x}Ca_xMnO_3$ $(0.0 \le x \le 0.5)$, Materials Chemistry and Physics 102 (2007) 47–52.

[24] C. Ettarh, A.K. Galwey, Thermal analysis of anhydrous mixtures of calcium nitrate and selected metal oxides, Thermochimica Acta 261 (1995) 125–139.
[25] Q. Zhou, B.J. Kennedy, Thermal expansion and structure of orthorhombic $CaMnO_3$, The Journal of Physics and Chemistry of Solids 67 (2006) 1595–1598.
[26] R.A. Young, The Rietveld Method, IUCr Monographs on Crystallography, vol. 5, , 1996, pp. 132–166.
[27] C.H. Yan, Z.G. Xu, F.X. Xheng, Z.M Wang, L.D. Sun, C.S. Liao, J.T. Jia, Nanophased $CoFe_2O_4$ prepared by combustion method, Solid State Communications 111 (1999) 287–291.
[28] B.D. Cullity, S.R. Stock, Elements of X-ray Diffraction, 3rd ed., Prentice-Hall Inc., 2001, pp. 167–171.
[29] Q. Zhou, B.J. Kennedy, Thermal expansion and structure of orthorhombic $CaMnO_3$, The Journal of Physics and Chemistry of Solids 67 (2006) 1595–1598.
[30] E. Dagotto, J. Burgy, A. Moreo, Nanoscale phase separation in colossal magnetoresistance materials: lessons for the cuprates?, Solid State Communications 126 (2003) 9–22
[31] D. Markovic, V. Kusigerski, M. Tadic, J. Blanusa, V. Antisari, V. Spasojevic, Magnetic properties of nanoparticle $La_{0.7}Ca_{0.3}MnO_3$ prepared by glycine-nitrate method without additional heat treatment, Scripta Materialia 59 (2008) 35–38.
[32] X.J. Fan, H. Koinuma, T. Hasegawa, Ferromagnetic correlation and metallic behavior in slightly electron-doped antiferromagnetic $CaMnO_3$, Physica B: Condensed Matter 329 (2003) 723–724.
[33] O. Peña, M. Bahout, K. Ghanimi, P. Duran, D. Gutierrez, C. Moure, Spin reversal and ferrimagnetism in (Gd, Ca)MnO_3, Journal of Mathematical Chemistry 12 (2002) 2480–2485.
[34] J.A. Mydosh, Spin Glasses: An Experimental Introduction, Taylor and Francis, London, 1993.